A common framework for the design optimization of fixed-wing, multicopter and VTOL UAV configurations

Félix Pollet, Scott Delbecq, Marc Budinger, Jean-Marc Moschetta, Jonathan Liscouët

33RD CONGRESS
OF THE INTERNATIONAL COUNCIL
OF THE AERONAUTICAL SCIENCES
STOCKHOLM, SWEDEN, 4-9 SEPTEMBER, 2022

ICAS 2022 SWEDEN

A COMMON FRAMEWORK FOR THE DESIGN OPTIMIZATION OF FIXED-WING, MULTICOPTER AND VTOL UAV CONFIGURATIONS

Félix Pollet[1], Scott Delbecq[1], Marc Budinger[2], Jean-Marc Moschetta[1] & Jonathan Liscouët[3]

[1]ISAE-SUPAERO, Université de Toulouse, France
[2]ICA, Université de Toulouse, ISAE-SUPAERO, MINES ALBI, UPS, INSA, CNRS, Toulouse, France
[3]Concordia University, 1455 De Maisonneuve Blvd., Montreal, QC H3G 1M8, Canada

Abstract

In recent years, unmanned aerial vehicles applications have grown in various fields. New design configurations have emerged to address these needs. This paper focuses on the multidisciplinary design optimization of three popular concepts of drones under a common framework: multicopters, fixed-wings, and the more recent fixed-wing VTOLs. Low-fidelity but computationally efficient models for drone sizing are proposed, some of them being shared by the different concepts. The models are integrated with a design optimization approach, and an efficient sizing methodology allows for reducing the problem complexity. This approach is instrumental because of the large number of design variables and contraints involved in the multidisciplinary design process. Examples of sizing results are provided to validate the methodology for fixed wing UAVs. In addition, a study case demonstrates the benefit of a common framework for comparing the performances of different drone concepts. A key finding is that the VTOL propulsion of the fixed-wing VTOLs must be carefully optimized to avoid an undesirable mass penalty.

Keywords: UAV, Drone, Multicopter, Fixed-wing, VTOL, Design optimization, MDO

1 Introduction

Unmanned aerial vehicles (UAVs) have been increasingly used in recent years to meet a diversifying industrial market. These flying vehicles cover a broad spectrum of applications: agriculture, transport of medical equipment, and aerial inspection among others [1–5]. To meet these needs, designers have developed and tested different concepts of drones. Multicopters, or multirotor drones, are rotorcraft composed of several propellers providing lift and thrust simultaneously, with the advantage of agility and precision. Multicopter configurations include quadcopters, hexacopters and octocopters with either one or two propellers per arm. In contrast, fixed-wing UAVs use surfaces for lift, while thrust is provided by one or several propellers. Many configurations for fixed-wing UAVs exist, but only the tail-aft configuration with a single engine is addressed in this paper. That is, the drone consists of wings, a fuselage, and an empennage mounted at its rear end. The propeller is located at the front of the fuselage. Finally, fixed-wing VTOL (FW-VTOL) drones are hybrid platforms combining a fixed-wing with the ability of vertical takeoff and landing (VTOL). The present paper covers the separate lift-thrust configuration, also known as quad-planes, where the forward flight uses a different powertrain compared to the hover flight. More precisely, four lifting propellers are attached to horizontal arms connected to the wings, as depicted in Figure 1c. UAVs can be powered by a wide range of sources such as batteries, fuel cells or combustion engines. The focus is here on battery-powered drones with electric powertrains.

As the applications of UAVs become more diverse, it becomes necessary to develop holistic design approaches with better technology integration, lower costs, and faster development time. A few solutions for UAV design exist, but none of them offers both comprehensive multidisciplinary modelling and coverage of multiple drone concepts. The popular web-based solutions eCalc [9] and flyEval [10] are used for evaluating the performance of multicopters, but no practical design optimization techniques are considered. Gatti [11] and Bershadsky [12] developed systematic approaches for sizing

Nomenclature

δ_{pro}	propeller clearance
Λ	sweep angle
λ	taper ratio
λ_f	fuselage fineness ratio
σ_{max}	maximum allowable stress
υ_{ht}	horizontal tail volume ratio
υ_{vt}	vertical tail volume ratio
a_{to}	takeoff acceleration
AR	aspect ratio
b_w	wing span
c	chord length
C_{D_0}	parasitic drag coefficient
C_f	skin friction coefficient
$C_{L_{max}}$	maximum lift coefficient
d_f	fuselage diameter
d_{out}	arm outer diameter
d_{pro}	propeller diameter
e	span efficiency factor
FF	shape form factor
h_{spar}	spar height
k_{arm}, k_{spar}	arms and spars aspect ratios
l_f	fuselage length
l_t	tail moment arm
M_{root}	bending moment at root
m_{uav}	total mass of the UAV
N_{pro}	number of propellers
q	dynamic pressure
S	area
S_{top}	top area of the airframe (projected)
S_{wet}	wetted area
t/c	thickness-to-chord ratio
T/W	thrust-to-weight ratio
t_{max}	flight endurance
t_{wing}	minimum wing thickness
V_v	rate of climb
V_{climb}	climb speed
V_{cruise}	cruise speed
V_{stall}	stall speed
W/S	wing loading
x_{cg}	center of gravity
x_{np}	neutral point

electric multicopter configurations by taking into account the mission profile and a few performance requirements. However, the scope of the models is limited to the propulsion system. The authors of CLOUDS [13–15] propose a similar solution for sizing UAVs with considerations for the main disciplines of aircraft design such as aerodynamics, weights, structures and propulsion. Although the CLOUDS solution is very efficient, the models are only applicable to multicopters. A preliminary sizing method for FW-VTOL drones is presented by Tyan [16] and An [17]. Yet, the use of empirical

(a) DJI Matrice 600 Pro [6] (b) Delair DT26 [7] (c) AeroVironment JUMP 20 [8]

Figure 1 – Multicopter, Fixed-Wing and FW-VTOL concepts

mass fractions limits the exploration of new configurations and technology improvements. In addition, no specific strategy is employed to solve the optimization singularities such as the mass calculation loop, which is time-consuming. Stahl presented a design and performance analysis tool for FW-VTOL drones in [18, 19], that relies on a comprehensive modelling of the UAV's systems and disciplines. Here again, no practical strategy is adopted to solve the design problem. The optimization is achieved through a statistical design of experiments, which makes it inefficient when many design variables are involved. Finally, the sizing of different drone concepts with a design optimization approach is addressed by Leng et al. [20, 21]. However, the focus is mainly on the aerodynamics.
The current paper covers the development of a multidisciplinary design optimization (MDO) methodology applied to fixed-wing, multicopter and FW-VTOL configurations. It relies on a comprehensive modelling of the main disciplines including geometries, propulsion, structures, aerodynamics and stability. In addition, the efficient formulation of the optimization problem significantly reduces the computational cost. The implementation of this methodology into a design tool allows for sizing and comparing different UAV concepts for similar specifications at a preliminary stage. The rest of this paper is organized as follows: Section 2 provides a set of design models for the main components and disciplines of electric UAVs. Section 3 presents an efficient sizing methodology that optimizes the vehicle with respect to the flight endurance or maximum takeoff weight. Finally, Section 4 provides examples of sizing results obtained with the methodology.

2 Design Models

The focus of this paper is on low-fidelity models. These models provide sufficiently good predictions for preliminary design while dramatically reducing computation time compared to higher fidelity models. In addition, the use of analytical design models facilitates the implementation of computationally efficient solutions for sizing.

2.1 UAV simulation model

The goal of the UAV simulation model is to derive the main quantities for the selection of the vehicle's components, based on a few sizing scenarios. We focus here on the two most important parameters affecting UAV performance: the thrust-to-weight ratios T/W and, when applicable, the wing loading W/S.

Wing loading

For UAVs with lifting surfaces, the wing loading is the vehicle's total weight divided by its wing area. The wing loading must be optimized depending on the application. High wing loadings lead to poor maneuverability, but improve performance at high speeds. Raymer [22] provides methods to estimate the wing loading required under various performance conditions. To maximize the range during cruise, in effect when flying at the speed for the maximum lift-to-drag ratio, the optimal wing loading must be such that:

$$(W/S)_{cruise} = q\sqrt{C_{D_0}/K} \tag{1a}$$

$$K = \frac{1}{\pi A R_w e} \tag{1b}$$

where $q = 0.5\rho_{air}V^2$ is the dynamic pressure at the selected airspeed V and air density ρ_{air}. AR_w is the wing's aspect ratio and C_{D_0} is the parasitic drag of the UAV. The span efficiency factor e for straight wings can be calculated as follows [22]:

$$e = 1.78(1 - 0.045AR_w^{0.68}) - 0.64 \tag{2}$$

Low-speed UAVs generally have wings with low sweep, as it provides better performance under these conditions. Consequently, the use of Equation 2 is extended to low sweep angles for which it remains a good approximation.
Optimizing the wing loading for cruise generally leads to small wings, and consequently a high stall speed. Although this issue is not critical for drones with lifting rotors, it can compromise the safety of a fixed-wing UAV. Given a required stall speed or, indirectly, an approach speed, the maximum wing loading not to be exceeded is expressed as [22]:

$$W/S \leq (W/S)_{stall} = qC_{L_{max}} \tag{3}$$

where $C_{L_{max}}$ is the maximum lift coefficient of the wing. For wings with a fairly high aspect ratio, $C_{L_{max}}$ can be approximated as 90% of the airfoil maximum lift coefficient $C_{l_{max}}$ [22].

Thrust-to-weight ratios
The thrust-to-weight ratios are used to size the propulsion system for the various flight scenarios. Endurance scenarios like hovering flight or cruise flight directly affect the battery selection through the required energy. Extreme criteria such as takeoff acceleration impact the sizing of the whole propulsion system.
The thrust requirements for a multicopter at takeoff, climb, hover and forward flight are presented in [23] and [24]. The equations are recalled in Equation 4 for convenience, where m_{uav} is the total mass of the UAV, a_{to} is the acceleration at takeoff and D_{climb}, D_{cruise} are the drag efforts to overcome.

$$(T/W)^{MR}_{hover} = 1 \tag{4a}$$

$$(T/W)^{MR}_{takeoff} = 1 + \frac{a_{to}}{g} \tag{4b}$$

$$(T/W)^{MR}_{climb} = 1 + \frac{D_{climb}}{m_{uav}g} \tag{4c}$$

$$(T/W)^{MR}_{cruise} = \sqrt{1 + \left(\frac{D_{cruise}}{m_{uav}g}\right)^2} \tag{4d}$$

When a UAV flies in a fixed-wing configuration, the thrust-to-weight ratios are calculated as follows [22]:

$$(T/W)^{FW}_{cruise} = \frac{qC_{D_0}}{W/S} + \frac{K}{q}.W/S \tag{5a}$$

$$(T/W)^{FW}_{climb} = \frac{V_v}{V_{climb}} + \frac{q}{W/S}.C_{D_0} + \frac{K}{q}.W/S \tag{5b}$$

where W/S is the wing loading and V_v is the rate of climb. Takeoff is assumed to be performed via a catapult that launches the UAV at a speed ten percent greater than the stall speed. Similarly to Equation 5b, the thrust-to-weight ratio for takeoff — or initial climb is expressed as:

$$(T/W)^{FW}_{takeoff} = \frac{V_v}{V_{takeoff}} + \frac{q}{W/S}.C_{D_0} + \frac{K}{q}.W/S \tag{6a}$$

$$V_{takeoff} = 1.1V_{stall} \tag{6b}$$

2.2 Estimation models for the electric propulsion system

The electric propulsion system (EPS) is composed of propellers, motors, electronic speed controllers (ESC) and batteries, connected by electrical wires. A set of estimation models for the propulsion

system, that is, models that return the main characteristics of the components from a few sizing parameters, is provided by Budinger et al. [25]. These estimation models are based on dimensional analysis. Such an approach provides a better understanding of the underlying physics compared to pure empirical models, which helps identify the performance drivers in the final design. The use of scaling laws makes it robust to scale changes and enables the exploration of new technologies, as only one reference value is needed. Finally, the continuous mathematical form of the estimation models facilitates the selection procedure of the components during the design process [23].
We assume in this paper that the models provided in [25] can be applied to both multirotor propulsion systems and fixed-wing propulsion systems with an appropriate change in the models' parameters where required. In particular, a new regression model for the performance of fixed-wing UAV propellers is obtained by applying the same methodology used for multirotor UAVs. The FW-VTOL configuration includes two separate propulsion systems sized from their respective flight scenarios.

2.3 Geometry

This section provides the main analytical models for the geometry of the drone concepts.

Multicopter

The arms supporting the propellers for multirotor drones are sized such that the propellers do not collide with each other, given a clearance distance. The top surface S_{top} and front surface S_{front} of the body frame are assumed to scale with the total mass m_{uav} of the vehicle [24]:

$$\frac{S_{top}}{S_{top,ref}} = \left(\frac{m_{uav}}{m_{uav,ref}}\right)^{2/3} \tag{7a}$$

$$\frac{S_{front}}{S_{front,ref}} = \left(\frac{m_{uav}}{m_{uav,ref}}\right)^{2/3} \tag{7b}$$

where the subscript $._{ref}$ refers to the properties of a reference multicopter. The derivation of Equation 7 assumes geometric similarity, i.e. the frame length ratios from one airframe to another are constant. A validation with commercially available multicopters can be found in [24].

Fixed-wing

For the fixed-wing parts, the surface S_w of the wing is first derived from the total mass of the UAV and the previously selected wing loading. The wingspan b_w and chords lengths c at various positions y of the wing are derived from the dimensionless aspect ratio AR_w and taper ratio λ_w, assuming a trapezoidal wing planform:

$$b_w = \sqrt{AR_w S_w} \tag{8a}$$

$$c(y) = \frac{2S_w}{(1+\lambda_w)b_w}\left[1 - \frac{1-\lambda_w}{b_w}|2y|\right] \tag{8b}$$

The areas of the stabilizing surfaces are obtained from the horizontal tail volume coefficient υ_{ht} and the vertical tail volume coefficient υ_{vt} introduced by Raymer [22]. These non-dimensional ratios compare the product of the stabilizing surfaces to the wing geometry, and are strongly linked to the aircraft stability (see Section 2.6).

$$\upsilon_{ht} = \frac{l_t S_{ht}}{c_{MAC_w} S_w} \tag{9a}$$

$$\upsilon_{vt} = \frac{l_t S_{vt}}{b_w S_w} \tag{9b}$$

Here, l_t is the tail moment arm, that is the distance between the quarter of the wing's mean aerodynamic chord (MAC) and the quarter of the tail's MAC. Here, the MAC is approximated by the mean geometric chord (MGC), which is a common assumption in aircraft design [26]. Typical values for homebuilt aircraft are 0.50 for υ_{ht} and 0.04 for υ_{vt} [22], but other values may be applied depending on

the application and stability requirements. The other geometrical parameters of the tails are derived similarly to the wing. However, lower aspect ratios will be preferred during optimization because the structural criterion is dominant over the aerodynamic criterion for these parts [27, 28].
Finally, the fuselage is made of a semi-spherical nose, a cylindrical mid-fuselage housing the batteries and the payload, and a conical rear-fuselage aft of the wing's trailing edge, as depicted in Figure 2. The total fuselage length is the sum of the wing position and the tail moment arm. Its maximum diameter is derived from a fineness ratio.

Fixed-wing VTOL
The VTOL propellers of a FW-VTOL drone must be located outside the high-turbulence area defined by the diameter of the fixed-wing propellers. Consequently, their distance from the axis of symmetry of the UAV must lie within the following range:

$$\left(\frac{d_{pro}^{FW}}{2}+\frac{d_{pro}^{MR}}{2}+\delta_{pro}\right)\leq y_{pro}^{MR}\leq\frac{b_w}{2} \tag{10}$$

where y_{pro}^{MR} are the locations of the propellers on the y-axis, d_{pro}^{FW} (d_{pro}^{MR}) is the diameter of the fixed-wing (multirotor) propellers, and δ_{pro} is the clearance distance. The location on the x-axis (i.e. along the fuselage and from the nose tip) is set such that the propellers do not collide or overlap with the wing. Therefore, the minimum length of the arms supporting the VTOL propellers is:

$$l_{arm}\geq c_{root_w}+y_{pro}^{MR}(\tan\Lambda_{TE_w}-\tan\Lambda_{LE_w})+(d_{pro}^{MR}+2\delta_{pro})\left(\frac{1}{\cos\Lambda_{TE_w}}+\frac{1}{\cos\Lambda_{LE_w}}\right) \tag{11}$$

where c_{root_w} is the wing root chord and Λ_{LE_w} (Λ_{TE_w}) is the sweep angle of the wing's leading edge (trailing edge).

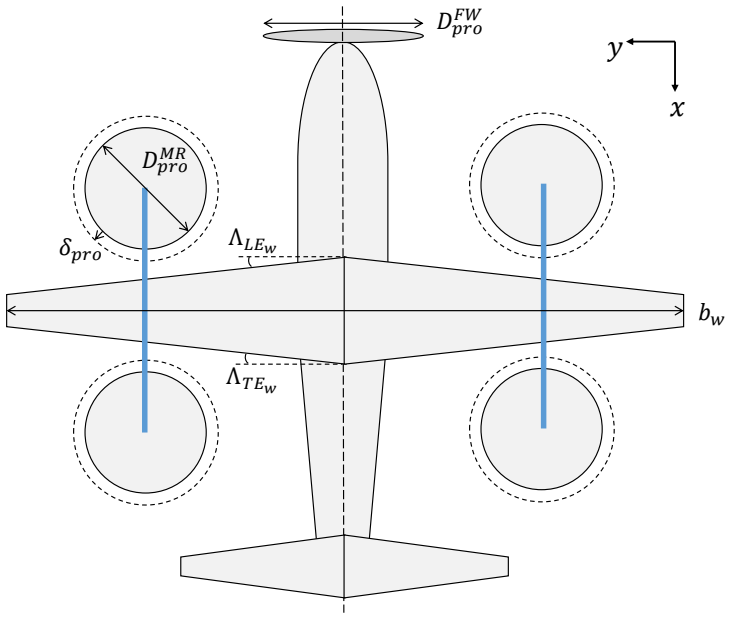

Figure 2 – VTOL propellers location for FW-VTOL geometry

2.4 Structures

The primary structures, that is, the arms supporting the VTOL propellers and the spars ensuring the wing's integrity, are sized using a bending stress calculation based on the maximum loads provided by the UAV simulation model.
The arms are represented by cantilever beams of length l_{arm} with a circular hollow section of diameters d_{in} and d_{out}, at the extremity of which a maximum load F_{max} corresponding to the takeoff thrust is

applied. The corresponding bending stress at the root is expressed as

$$\sigma_{root} = \frac{M_{root}}{I}\frac{d_{out}}{2} = \frac{32 d_{out} M_{root}}{\pi(d_{out}^4 - d_{in}^4)} = \frac{32 M_{root}}{\pi d_{out}^3 (1 - k_{arm}^4)} \leq \sigma_{max} \tag{12a}$$

$$M_{root} = \frac{T_{takeoff}}{N_{pro}^{MR}} l_{arm} \tag{12b}$$

where I is the moment of inertia of the beam, k_{arm} is the ratio of inner diameter to outer diameter, and N_{pro}^{MR} is the number of VTOL propellers. The bending stress must not exceed the maximum allowable stress σ_{max} of the material.
An I-beam model is used for the wing spars, as I-shapes provide good structural properties at the cost of higher manufacturing complexity. However, other options such as hollow square beams will be implemented in future works. In a first approach, it is assumed that the bending moment is entirely reacted by the flanges of the I-beam. Equation 12a is transformed into:

$$\sigma_{root} = \frac{M_{root} K_{flange}(1 + k_{spar})}{h_{spar}^3 k_{spar}^2 (1 + k_{spar}^2/3)} \leq \sigma_{max} \tag{13}$$

where K_{flange} is the ratio of the flanges' thickness to the flanges' length, generally in the order of 0.1 and taken constant here. k_{spar} is the flanges' thickness divided by the distance h_{spar} between the two flanges. Two sizing cases are considered for the spars, as they must support the aerodynamic forces acting on the wing and, for FW-VTOL drones, the vertical take-off thrust. The aerodynamic load on each half-wing is obtained from the equilibrium in cruise conditions and a load factor n_z. It is assumed to be applied at the wing's MAC location [22]. The thrust generated by the VTOL propellers at takeoff is transmitted to the spars via the arms. The point of application of this load is equal to the y-location of the arms, y_{pro}^{MR}. The resulting bending moments for each half-wing are:

$$M_{root}^{FW} = \frac{n_z m_{uav} g}{2} y_{MAC} \tag{14a}$$

$$M_{root}^{MR} = \frac{T_{takeoff}}{2} y_{pro}^{MR} \tag{14b}$$

Finally, the height of the spars must not exceed the minimum wing thickness:

$$h_{spar} \leq t_{wing} \tag{15}$$

For simplicity, torsion and shear stresses are neglected for sizing the wing, limiting to applications with low speeds (i.e., low control surface hinge moments). A conservative approach is adopted for sizing the ribs and the skin. These components are sized from their materials properties (e.g. balsa wood for the ribs) and wing's geometry, with a constant thickness. The spacing of the ribs is assumed to be approximately one half of the mean aerodynamic chord [26].
The loads applied to the tails and the fuselage are neglected. The weights of these components are obtained directly from the densities of the materials they are made of, for example, monolithic carbon-fiber-reinforced polymers (CFRP).

2.5 Aerodynamics

The drag coefficient C_D and lift coefficient C_L of the whole UAV are two important parameters impacting the flight performance, as they relate to the aerodynamic forces applying to the vehicle. In particular, the calculations of the wing loading and thrust-to-weight ratios introduced in Section 2.1 require the value of the parasitic drag coefficient C_{D_0}. The aerodynamics models presented here are reduced to the description of this parameter.
The aerodynamics of multicopters in forward flight have been introduced by the authors in [24]. It consists of a fixed drag coefficient and the calculation of the airframe's projected areas. The reason for having a user-defined drag coefficient is that the shape of the frame is largely dependent on the application and payload, which a generic model will not be able to properly assess.
For fixed-wing and FW-VTOL concepts, the parasitic drag C_{D_0} is computed with a component buildup

method [22], assuming no aerodynamic interaction between the different parts of the airframe, and with the propellers. It consists of estimating the parasitic drag of each part of the UAV with an equivalent flat-plate skin friction coefficient and a shape form factor:

$$C_{D_0} = \frac{1}{S_w}\left(\sum_{i=1}^{N_{surfaces}} C_{f,i} FF_i S_{wet,i} + C_{D_{pro}}^{MR} S_{pro}^{MR}\right) \tag{16}$$

Fixed-wing parts

The flat-plate skin friction coefficient C_f is calculated assuming a complete turbulent flow and taking into account compressibility effects [29]:

$$C_f = \frac{0.455}{(\log_{10} Re)^{2.58}(1+0.144M^2)^{0.65}} \tag{17}$$

The shape form factors FF are calculated as proposed by Raymer [22]:

$$FF_{fuselage} = 1 + \frac{60}{\lambda_f^3} + \frac{\lambda_f}{400} \tag{18a}$$

$$FF_{wings} = \left[1 + \frac{0.6}{(x/c)_m}\left(\frac{t}{c}\right) + 100\left(\frac{t}{c}\right)^4\right]\left[1.34M^{0.18}(\cos\Lambda_m)^{0.28}\right] \tag{18b}$$

where λ_f is the fuselage fineness ratio and t/c is the thickness-to-chord ratio of the wing's airfoil. The parameter $(x/c)_m$ is the chordwise location of the airfoil maximum thickness and Λ_m is the sweep at this location.

The wetted areas of the wing and tails are taken as twice their area, and the fuselage wetted area is calculated from its diameter d_f and length l_f [28]:

$$S_{wet_{fuselage}} = \pi d_f l_f \left(1 - \frac{2}{\lambda_f}\right)^{2/3}\left(1 + \frac{1}{\lambda_f^2}\right) \tag{19}$$

Stopped propellers

The term $C_{D_{pro}}^{MR}$ in Equation 16 refers to the parasitic drag originating from the stopped propellers of the multirotor propulsion system, specifically for FW-VTOL configurations in forward flight. In feather position, when the blades are parallel to the airflow, Hoerner [30] provides a value of 0.1 for the drag coefficient of a single blade. This value is corrected with a solidity ratio to obtain the parasitic drag coefficient at the propeller scale:

$$C_{D_{pro}}^{MR} = 0.1\sigma_{pro} = 0.1\frac{N_{blades} c_{blade}}{\pi r_{pro}} \tag{20}$$

Based on the geometry of three-bladed APC propellers [31] retrieved from UIUC data site [32], a mean value of 0.15 is adopted for the solidity ratio.

2.6 Stability

The longitudinal static stability of the fixed-wing and FW-VTOL concepts is assessed by the static margin of the UAV. The static margin is the relative distance between the centre of gravity of the UAV and the neutral point. A centre of gravity located ahead of the neutral point results in a positive static margin and a stable configuration. The centre of gravity x_{cg} of the UAV is estimated from the individual masses and positions of the components. Among others, it is assumed that the batteries are centred at the wing position. The centre of gravity of the lifting surfaces is approximated by the centre of mass of the airfoil at the MAC position, which is located at 40% of the chord for most NACA airfoils.

The neutral point represents the most-aft position of the centre of gravity before the UAV becomes unstable. At neutral point, the pitching moment of the UAV is zero. Solving the equation of the pitching moment for the neutral point yields [26]:

$$x_{np} = x_{ac} + c_{MAC_w} \upsilon_{ht} \frac{C_{L_{\alpha_{ht}}}}{C_{L_{\alpha_w}}}\left(1 - \frac{\partial\varepsilon}{\partial\alpha}\right) \tag{21}$$

The contribution of the fuselage in neglected in Equation 21. The wing's aerodynamic centre (ac) at low Mach numbers is located at the quarter-chord of the MAC [22]:

$$x_{ac} = x_{MAC/4} \tag{22}$$

The lift curve slopes C_{L_α} of the 3-dimensional wing and horizontal tail are calculated with the Prandtl's lifting-line theory:

$$C_{L_\alpha} = \frac{C_{l_\alpha}}{1 + \frac{C_{l_\alpha}}{\pi e AR}} = \frac{2\pi}{1 + \frac{2\pi}{\pi e AR}} \tag{23}$$

The ε term in Equation 21 is the downwash at the tail, originating from the trailing vortex behind the wing. The downwash slope with respect to the angle of attack is determined as follows:

$$\frac{\partial \varepsilon}{\partial \alpha} = \frac{2C_{L_{\alpha_w}}}{\pi e AR_w} \tag{24}$$

Finally, the static margin resulting from the calculations of the centre of gravity and the neutral point is obtained as:

$$SM = \frac{x_{np} - x_{cg}}{c_{MAC}} \tag{25}$$

3 Sizing Procedure and Design Optimization

A multidisciplinary design optimization (MDO) approach is adopted to solve the design problem. Because of the high number of variables involved, the optimization process can be computationally expensive. However, the application of an efficient sizing methodology as presented by Delbecq et al. [23] can significantly reduce the problem complexity. In particular, the Normalized Variable Hybrid (NVH) formulation approach is implemented to solve the multidisciplinary couplings and singularities such as algebraic loops [33]. The sizing methodology applied in [23] to multicopter drones shows a significant improvement of the computational cost compared to the non-reformulated problem, while providing accurate results. We propose here to extend the scope of the methodology developed in [23, 24] to fixed-wing and FW-VTOL UAVs.

3.1 Initial problem formulation

The optimization problem is defined by a single objective function, a set of design variables and several constraints. In this study, the objective function is either the flight endurance t_{max} of the drone or its total mass m_{uav}. The latter is the most frequently used objective in the optimization of aerial vehicles, as this parameter is directly linked to mission efficiency and vehicle cost [34].
For conciseness, only the optimization of the FW-VTOL concept is presented and discussed in this section. The optimization problems for fixed-wings and multicopters are obtained by replacing or removing the unnecessary design variables and constraints. The initial optimization parameters for FW-VTOL drones are provided in Table 1. A total of 25 design variables and 35 constraints are defined. The rest of this section focuses on the application of principles to reduce the problem complexity.

3.2 Monotonicity analysis

The first step of the efficient methodology presented in [23] is the application of the First Monotonicity Principle (MP1) to remove a number of inequality constraints. This principle, introduced by Papalambros and Wilde in [35], enables identifying the critical constraints of the problem, in effect the constraints that are the only ones to bound the objective function with respect to a design variable.

Table 1 – Initial optimization problem.

	Parameter	Description
Design variables	W/S	Wing loading
	AR_w, AR_{ht}, AR_{vt}	Aspect ratios of the wing and tails
	λ_w	Taper ratio of the wing
	$x_{MAC/4}$	Wing location w.r.t. nose tip
	l_t	Tail moment arm
	y_{pro}^{MR}	Location on y-axis of the VTOL propellers
	l_{arm}	Arms length
	d_{out}, h_{spar}	External dimensions of the arms and spars
	k_{arm}, k_{spar}	Aspect ratios of the arms and spars
	$\underline{x_{eps}}$	Set of 9 design variables per propulsion system [23, 24]
Constraints	$W/S \leq (W/S)_{stall}$	Constraint on the stall speed
	$SM_{req} \leq SM$	Constraint on the static margin
	$V_{bat} + V_{pay} \leq V_f$	Constraint on the fuselage volume
	$g_1(y_{pro}^{MR}) \leq 0$	Constraint on the minimum y-location of VTOL propellers
	$g_2(y_{pro}^{MR}) \leq 0$	Constraint on the maximum y-location of VTOL propellers
	$g_3(l_{arm}) \leq 0$	Constraint on the minimum arms' length
	$\sigma_{root_{arm}} \leq \sigma_{max}$	Constraint on the arms' bending stress
	$h_{spar} \leq t_{wing}$	Constraint on the spars' height
	$\sigma_{root_{spar}} \leq \sigma_{max}$	Set of 2 constraints on the spars' bending stress
	$\underline{g(x_{eps})} \leq 0$	Set of 20 constraints per propulsion system [23, 24]
	$E_{mission} \leq E_{bat}$	Constraint on the battery energy
	$m_{uav} \leq m_{uav,req}$	Constraint on the maximum total mass
Objectives	m_{uav}	Total mass of the UAV
	t_{max}	Flight endurance

The critical constraints can be turned into equalities and removed from the problem formulation. Delbecq [23] provides a detailed explanation on how to carry out a monotonicity analysis. By applying this strategy to our case study, the following critical constraints are detected:

Equation 11 critical w.r.t. l_{arm}

$$\longrightarrow l_{arm} = c_{root_w} + y_{pro}^{MR}(\tan\Lambda_{TE_w} - \tan\Lambda_{LE_w}) + (d_{pro}^{MR} + 2\delta_{pro})\left(\frac{1}{\cos\Lambda_{TE_w}} + \frac{1}{\cos\Lambda_{LE_w}}\right) \tag{26a}$$

Equation 12a critical w.r.t. d_{out}

$$\longrightarrow d_{out} = \left(\frac{32M_{root}}{\pi\sigma_{max}(1-k_{arm}^4)}\right)^{1/3} \tag{26b}$$

The two initial inequality constraints are therefore replaced by equalities and removed from the optimization problem formulation.

3.3 Normalized Variable Hybrid formulation

The optimization problem can be further reduced by detecting and solving the mathematical singularities in the initial set of equations. The problem defined in Section 3.1 contains algebraic loops and over-constrained sets of equations.

Algebraic loops

An example of algebraic loop is the mass calculation. The propulsion systems and the structures are sized from the thrust requirements, and the thrust calculations require the total mass of the UAV to be known. Yet, the latter is computed from the contribution of the individual masses, thus leading to a feed-back loop. Algebraic loops can be solved by a fixed-point algorithm, but it has a significant impact on the computational effectiveness. Following the Normalized Variable Hybrid (NVH) formulation introduced in [33], the mass loop is broken by setting an initial guess for the total

mass, assumed to be a multiple of the known payload mass:

$$m_{uav,guess} = k_M m_{payload} \tag{27}$$

with k_M an input variable within the range $[1,\infty)$. A consistency constraint is added to the optimization problem to ensure that the initial guess converges to the actual mass after several iterations:

$$m_{uav,guess} \geq m_{uav} \tag{28}$$

A similar issue is encountered with the drag calculation. The parasitic drag coefficient is calculated from the geometry of the airframe and, for FW-VTOL drones, the diameter of the VTOL propellers. However, the propulsion systems are sized from the thrust requirements, derived with the parasitic drag coefficient. Although this feed-back loop can be resolved by re-organizing the equations in a specific order, it would break the disciplines-oriented approach. Therefore, an initial guess of the parasitic drag coefficient is obtained from a reference value, and a constraint is added to ensure that both the initial guess and the final value tend to a unique solution:

$$C_{D_0,guess} = k_{C_{D_0}} C_{D_0,ref} \tag{29a}$$

$$C_{D_0,guess} = C_{D_0} \tag{29b}$$

In practice the equality constraint is treated as a pair of inequalities for better numerical handling.
Finally, an algebraic loop is found when computing the thrust-drag equilibrium in climbing flight. The projected top area of the UAV is required for the drag calculation but is only accessible as an output of the geometry module as it requires the wing, tails and fuselage to be sized. For the FW-VTOL drones, an initial guess of the top area is obtained from the wing loading and the UAV's mass:

$$S_{top,guess} = k_S \frac{m_{uav} g}{W/S} \tag{30a}$$

$$S_{top,guess} \geq S_{top} \tag{30b}$$

Over-constrained sets of equations

Over-constrained singularities are found in the initial set of equations. For FW-VTOL drones, the y-location of the VTOL propellers is defined from two inequalities (Equation 10) and one undetermined parameter, y_{pro}^{MR}. To obtain a non-singular problem, one of the inequalities is moved to the problem constraints. The remaining inequality is transformed to an equality by introducing a degree of freedom $k_{y_{pro}}$:

$$y_{pro}^{MR} = k_{y_{pro}} \left(\frac{d_{pro}^{FW}}{2} + \frac{d_{pro}^{MR}}{2} + \delta_{pro} \right) \tag{31a}$$

$$y_{pro}^{MR} \leq \frac{b_w}{2} \tag{31b}$$

where $k_{y_{pro}}$ is a normalized input within the range $[1,\infty)$. This allows to have a design variable whose lower bound is independent of the application.
The structural sizing of the spars sets outs two equations (Equations 13, 14) with two undetermined parameters, h_{spar} and k_{spar}. The resolution strategy involves moving one of the inequalities to the constraints of the problem, and introducing a normalized design variable k_σ to transform the second into an equality.

$$\sigma_{root}^{FW} = k_\sigma \sigma_{max} \tag{32a}$$

$$\sigma_{root}^{MR} \leq \sigma_{max} \tag{32b}$$

Or, expressing Equation 32a in terms of the spars' height:

$$h_{spar} = k_{h_{spar}} \left(\frac{M_{root}^{FW} K_{flange}(1+k_{spar})}{\sigma_{max} k_{spar}^2 (1+k_{spar}^2/3)} \right)^{1/3} \tag{33a}$$

$$\sigma_{root}^{MR} \leq \sigma_{max} \tag{33b}$$

with $k_{h_{spar}}$ an oversizing coefficient within the range $[1, \infty)$.

The introduction of normalized design variables, whose bounds are independent of the application, improves the numerical solution accuracy and convergence properties [33]. For the same reasons, the design variables representing the wing loading, the tail moment arm and the wing position are replaced by introducing normalized variables:

$$W/S = k_{WS}(W/S)_{cruise} \tag{34a}$$
$$l_t = k_t b_w \tag{34b}$$
$$x_{MAC/4} = k_w b_w \tag{34c}$$

The design variables k_{WS}, k_t and k_w are used to scale the physical parameters with respect to an initial guess.

3.4 Reduced problem formulation and implementation

The final optimization problem is summarized in Table 2. A visual summary of the MDO architecture is provided in Figure 3 with an extended design structure matrix (XDSM) [36]. In addition to better handling of algebraic loops, the number of design variables has been reduced from 25 to 23, and the number of constraints from 35 to 28.

Table 2 – Reduced optimization problem.

	Parameter	Description
Design variables	k_{WS}	Sizing coefficient on the wing loading
	AR_w, AR_{ht}, AR_{vt}	Aspect ratios of the wing and tails
	λ_w	Taper ratio of the wing
	k_w	Sizing coefficient on the wing position
	k_t	Sizing coefficient on the tail moment arm
	$k_{y_{pro}}$	Sizing coefficient on the y-location of VTOL propellers
	$k_{h_{spar}}$	Sizing coefficient on the spars' height
	k_{arm}, k_{spar}	Aspect ratios of the arms and spars
	$\underline{x_{eps}}$	Set of 9 design variables per propulsion system [23, 24]
	k_M	Oversizing coefficient on the load mass
	$k_{C_{D_0}}$	Sizing coefficient on the parasitic drag coefficient
	k_S	Oversizing coefficient on the wing surface
Constraints	$W/S \leq (W/S)_{stall}$	Constraint on the stall speed
	$SM_{req} \leq SM$	Constraint on the static margin
	$V_{bat} + V_{pay} \leq V_f$	Constraint on the fuselage volume
	$y_{pro}^{MR} \leq b_w/2$	Constraint on the maximum y-location of VTOL propellers
	$h_{spar} \leq t_{wing}$	Constraint on the spars' height
	$\sigma_{root}^{MR} \leq \sigma_{max}$	Constraint on the spars' bending stress during VTOL
	$\underline{g}(\underline{x_{eps}}) \leq 0$	Set of 17 constraints per propulsion system [23, 24]
	$E_{mission} \leq E_{bat}$	Constraint on the battery energy
	$m_{uav} \leq m_{uav,req}$	Constraint on the maximum total mass
	$m_{uav} \leq m_{uav,guess}$	Consistency constraint on the total mass
	$C_{D_0,guess} = C_{D_0}$	Consistency constraint on the parasitic drag coefficient
	$S_{top} \leq S_{top,guess}$	Consistency constraint on the top (projected) area
Objectives	m_{uav}	Total mass of the UAV
	t_{max}	Flight endurance

The design optimization is implemented in FAST-OAD [37], an open-source framework for rapid overall aircraft design based on OpenMDAO [38]. The object-oriented framework, written in Python, allows easy switching between the models and adding or removing disciplines to match the desired

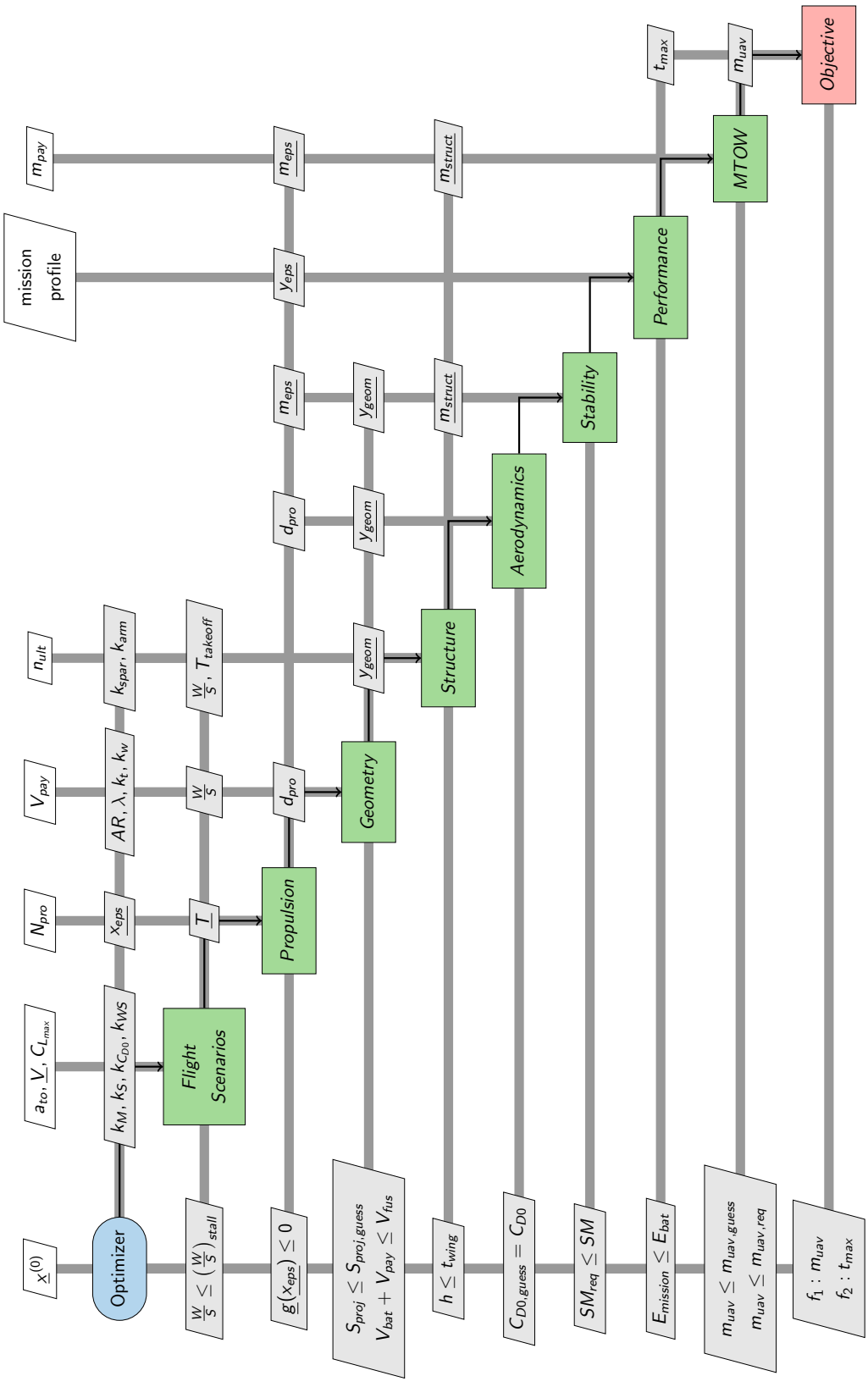

Figure 3 – XDSM diagram for FW-VTOL drones optimization.

drone concept. The continuous nature of the models involved in the sizing process motivates the use of a gradient-based optimizer, SLSQP [39]. This optimizer offers a shorter computation time compared to other global optimization algorithms. The algorithm performances for typical optimization problems using a 1.8 GHz quad-core processor are provided in Table 3.

Table 3 – Algorithm performances for different concepts of drones.

	Multirotor	Fixed-Wing	FW-VTOL
Number of function evaluations	101	139	129
Number of iterations	55	81	115
Resolution time (s)	4.1	14.2	21.8

4 Sizing results

A validation of the sizing tool for multicopter UAVs is provided in [23] and extended to take into account cruise flight in [24]. The wide variety of materials and technologies used for fixed-wing and FW-VTOL UAVs and the lack of extensive data on existing vehicles makes it difficult to provide a comprehensive validation of these concepts. However, we propose here to validate the sizing of fixed-wing UAVs based on a high-level characteristic easily accessible from manufacturers' data: the product of payload mass and endurance as a function of the total mass.

Examples of sizing results for five drones of different scales are depicted in Figure 4 and compared with existing vehicles [7, 40–51]. The drones are sized for a constant share of payload mass, equal to 20% of the total mass. A fixed mass is added to account for the flight management system and the communication systems. In addition, the same technological and material assumptions are applied to the five designs. Also provided in Figure 4 is the sizing correlation derived by D. Verstraete et al. [52] on the basis of 230 battery-powered fixed-wings introduced in the market before 2017.

The sizing results are consistent with the market trends, although they seem optimistic for small UAVs compared to Verstraete's regression. However, a great disparity is observed within the existing fixed-wings on the market. This is explained by the multitude of technological choices and materials available, in connection with economic factors. The low regression coefficient from Verstraete's correlation, equal to 0.827, highlights this phenomenon.

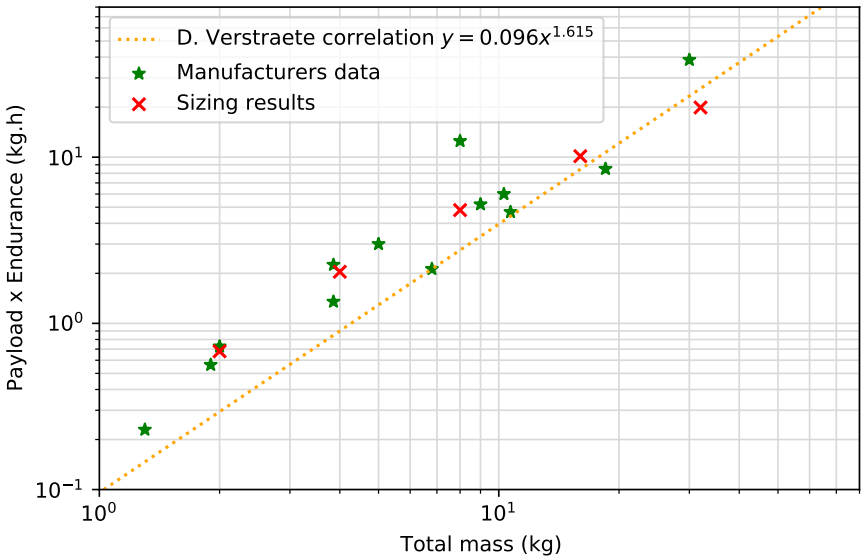

Figure 4 – Payload-endurance product as a function of total mass

The relevance of a common framework for sizing different concepts of drones is now illustrated with a study case. Table 4 provides sizing examples for a multicopter, a fixed-wing and a FW-VTOL drone, obtained with the same design tool. The UAVs are sized to carry a 3 kg payload at a cruise speed of 16 m/s while maximizing the cruise endurance. Predictably, the hexacopter configuration has less flight autonomy than its counterparts due to its lack of lifting surfaces. A drastic decrease in cruise endurance can also be observed for the FW-VTOL compared to the fixed-wing configuration. One of the reasons is that the VTOL propulsion system causes additional drag, which slightly increases energy consumption. But the main cause is the mass allocated to the VTOL propulsion system

which limits the amount of energy that can be carried to accomplish the mission. Therefore, future work should focus on optimizing the VTOL propulsion to reduce the mass penalty. In particular, the battery and the motors are the heaviest components of the propulsive chain [25]. Since the takeoff scenario is the main sizing driver for the VTOL propulsion, battery technologies providing high power densities will be preferred. The main criteria influencing the motors' size are the thermal aspects [25]. Consequently, a trade-off between the duration of maximum torque scenario and the motors' losses must be found to minimize the overall weight.
Finally, the structures account for a large part of the total mass, which underlines the importance of materials selection and structural optimization.

Table 4 – Sizing examples

		Hexacopter	FW-VTOL	Fixed-Wing
Inputs	Payload mass	3 kg	3 kg	3 kg
	Payload volume	0.015 m^3	0.015 m^3	0.015 m^3
	Total mass	15 kg	15 kg	15 kg
	Cruise speed	16 $m.s^{-1}$	16 $m.s^{-1}$	16 $m.s^{-1}$
	Climb speed / Rate of climb	3 $m.s^{-1}$	14 $m.s^{-1}$ / 3 $m.s^{-1}$	14 $m.s^{-1}$ / 3 $m.s^{-1}$
	Stall speed	-	13 $m.s^{-1}$	12.5 $m.s^{-1}$
	Vertical takeoff acceleration	0.8 g	0.3 g	-
	Materials	Carbon/fiberglass composites, balsa wood, foam		
Outputs	Max. cruise endurance	33 min	85 min	171 min
	Max. cruise distance	31.8 km	81.8 km	164.2 km
	Wing area	-	1.2 m^2	1.3 m^2
	Wing span	-	4.1	4.3
	Wing aspect ratio	-	14.1	14.1
	Taper ratio	-	1.0	1.0
	Fuselage length	-	1.6 m	1.7
	Footprint (length $\times$ width)	1.9 m^2	6.6 m^2	7.2 m^2
	Parasitic drag coefficient	0.5*	0.031	0.023
	Battery power in cruise	2067 W	211 W	178 W
	Battery energy**	1428 Wh	374 Wh	635 Wh
	FW propeller diameter	-	0.68 m	0.72 m
	MR propellers diameter	0.46 m	0.48 m	-
	Structures mass fraction	15%	44%	46%
	FW propulsion mass fraction	-	23%	35%
	MR propulsion mass fraction	65%	13%	-

* Drag coefficient for multirotor drones is a fixed input (see Section 2.5).
** Including a 20% energy reserve. Excluding VTOL battery for FW-VTOL configuration.

5 Conclusions

This paper introduces a design optimization methodology for multicopter, fixed-wing and FW-VTOL drones. Design models for the different disciplines (geometry, structures, aerodynamics, propulsion and stability) are provided, and an optimization problem is formulated. The complexity of the problem is reduced through the application of two methods: the monotonicity analysis and the NVH formulation. These strategies enable to remove a number of constraints and design variables without affecting the results, and to solve algebraic loops more efficiently. The implementation of the methodology into a sizing tool shows very low resolution times, making it suitable for preliminary design. Moreover, the formulation of the optimization problem introduces design variables whose bounds are independent of the application. Together with the previously presented models, this provides a design tool that is valid for a wide range of UAVs. The validity of the methodology is demonstrated for fixed-wings by comparing sizing results with existing drones. In addition, a first insight of the tool's ability to compare different concepts is provided through a case study. The results show limited benefit of the

FW-VTOL configuration over the multirotor due to the mass penalty of the dual propulsion system. Improving the FW-VTOL performance would require further optimization of the VTOL propulsion system by implementing new design models (for example, electric motor thermal model) and carefully selecting the power source (high-power batteries). Finally, the sizing tool could be further improved by refining the structural models and selecting the appropriate materials, as the structures account for a large share of the total mass. For example, taking into account wing torsion and empennage loads would provide more accurate results.

6 Contact Author Email Address

mailto: felix.pollet@isae-supaero.fr

7 Acknowledgements

This research was funded by ISAE-SUPAERO and INSA Toulouse, with the financial supports of Mitacs, under the Globalink Research Award, and ISAE-SUPAERO Foundation.

8 Copyright Statement

References

[1] Vu, N. A., Dang, D. K., and Le Dinh, T., "Electric propulsion system sizing methodology for an agriculture multicopter," *Aerospace Science and Technology*, vol. 90, pp. 314–326, 2019.

[2] Lamptey, E. and Serwaa, D., "HighTech and Innovation Journal The Use of Zipline Drones Technology for COVID-19 Samples Transportation in Ghana," *HighTech and Innovation Journal*, vol. 1, 2020.

[3] Metni, N. and Hamel, T., "A UAV for bridge inspection: Visual servoing control law with orientation limits," *Automation in Construction*, vol. 17, pp. 3–10, Nov. 2007.

[4] Shafiee, M., Zhou, Z., Mei, L., Dinmohammadi, F., Karama, J., and Flynn, D., "Unmanned Aerial Drones for Inspection of Offshore Wind Turbines: A Mission-Critical Failure Analysis," *undefined*, 2021.

[5] Videras Rodríguez, M., Melgar, S. G., Cordero, A. S., and Márquez, J. M. A., "A Critical Review of Unmanned Aerial Vehicles (UAVs) Use in Architecture and Urbanism: Scientometric and Bibliometric Analysis," *Applied Sciences*, vol. 11, p. 9966, Oct. 2021.

[6] "DJI Matrice 600 Pro." dji.com/matrice600-pro.

[7] "DT26 Open-Payload." delair.aero/delair-commercial-drones/dt26-open-payload/.

[8] "AeroVironment Jump 20." avinc.com/uas/jump-20.

[9] "eCalc." `https://www.ecalc.ch`.

[10] "Flight Evaluation." `https://flyeval.com/`.

[11] Gatti, M., "Complete Preliminary Design Methodology for Electric Multirotor," *J. Aerosp. Eng.*, p. 15, 2017.

[12] Bershadsky, D., Haviland, S., and Johnson, E. N., "Electric Multirotor UAV Propulsion System Sizing for Performance Prediction and Design Optimization," in *57th AIAA/ASCE/AHS/ASC Structures, Structural Dynamics, and Materials Conference*, (San Diego, California, USA), American Institute of Aeronautics and Astronautics, Jan. 2016.

[13] Lim, D., Kim, H., and Yee, K., "Mission-oriented performance assessment and optimization of electric multirotors," *Aerospace Science and Technology*, vol. 115, p. 106773, 2021.

[14] Lim, D., Kim, H., Lee, B., and Yee, K., "Unified framework for analysis and design optimization of a multirotor unmanned aerial vehicle," 2018.

[15] Oh, S., Kim, M., Kim, H., Lim, D., Yee, K., and Kim, D., "The Solution Development for Performance Analysis and Optimal Design of Multicopter-type Small Drones," in *2020 International Conference on Unmanned Aircraft Systems (ICUAS)*, pp. 975–982, Sept. 2020. ISSN: 2575-7296.

[16] Tyan, M., Nguyen, N. V., Kim, S., and Lee, J.-W., "Comprehensive preliminary sizing/resizing method for a fixed wing – VTOL electric UAV," *Aerospace Science and Technology*, vol. 71, pp. 30–41, 2017.

[17] An, J.-H., Kwon, D.-Y., Jeon, K.-S., Tyan, M., and Lee, J.-W., "Advanced Sizing Methodology for a Multi-Mode eVTOL UAV Powered by a Hydrogen Fuel Cell and Battery," p. 26, 2022.

[18] Stahl, P., Seren, T., Roessler, C., and Hornung, M., *Development and Performance Comparison of Optimized Electric Fixed-Wing VTOL UAV Configurations*. Nov. 2018.

[19] Stahl, P., Roessler, C., and Hornung, M., "Performance and Life Cycle Cost Comparison of Optimized Fixed-Wing VTOL UAV Configurations," p. 13 pages, 2020. Artwork Size: 13 pages Medium: application/pdf Publisher: Deutsche Gesellschaft für Luft- und Raumfahrt - Lilienthal-Oberth e.V. Version Number: 1.0.

[20] Yuchen, L., "Aerodynamic design of long endurance convertible UAV," p. 189, 2020.

[21] Fayez, K., Leng, Y., Jardin, T., Bronz, M., and Moschetta, J.-M., "Conceptual Design for Long-Endurance Convertible Unmanned Aerial System," in *AIAA Scitech 2021 Forum*, American Institute of Aeronautics and Astronautics, 2021.

[22] Raymer, D. P., *Aircraft Design: A Conceptual Approach*. American Institute of Aeronautics and Astronautics, Incorporated, 2018.

[23] Delbecq, S., Budinger, M., Ochotorena, A., Reysset, A., and Defay, F., "Efficient sizing and optimization of multirotor drones based on scaling laws and similarity models," *Aerospace Science and Technology*, vol. 102, p. 105873, July 2020.

[24] Pollet, F., Delbecq, S., Budinger, M., and Moschetta, J.-M., "Design optimization of multirotor drones in forward flight," Sept. 2021.

[25] Budinger, M., Reysset, A., Ochotorena, A., and Delbecq, S., "Scaling laws and similarity models for the preliminary design of multirotor drones," *Aerospace Science and Technology*, vol. 98, p. 105658, Mar. 2020.

[26] Gudmundsson, S., *General Aviation Aircraft Design: Applied Methods and Procedures*. Saint Louis: Elsevier Science & Technology, 1st ed. ed., 2013. Book Title: General Aviation Aircraft Design.

[27] Gomez-Rodriguez, A., Sanchez-Carmona, A., Garcia-Hernandez, L., and Cuerno-Rejado, C., "Prelimi-

nary Correlations for Remotely Piloted Aircraft Systems Sizing," *Aerospace*, vol. 5, p. 5, Jan. 2018.

[28] Torenbeek, E., *Synthesis of Subsonic Airplane Design: An introduction to the preliminary design of subsonic general aviation and transport aircraft, with emphasis on layout, aerodynamic design, propulsion and performance*. Springer Science & Business Media, Sept. 1982.

[29] Prandtl, L. and Schlichting, H., "The Resistance Law for Rough Plates," Jan. 1934.

[30] Hoerner, S. F., "Fluid-Dynamic Drag," p. 455.

[31] "APC Propellers." apcprop.com.

[32] Brandt, J., Deters, R., Ananda, G., Dantsker, O., and Selig, M., "UIUC Propeller Database, Vols 1-3."

[33] Delbecq, S., Budinger, M., and Reysset, A., "Benchmarking of monolithic MDO formulations and derivative computation techniques using OpenMDAO," 2020.

[34] Papageorgiou, A., Tarkian, M., Amadori, K., and Ölvander, J., "Multidisciplinary Design Optimization of Aerial Vehicles: A Review of Recent Advancements," 2018.

[35] Papalambros, P. Y. and Wilde, D. J., *Principles of Optimal Design: Modeling and Computation*. Cambridge University Press, July 2000.

[36] Lambe, A. B. and Martins, J. R. R. A., "Extensions to the design structure matrix for the description of multidisciplinary design, analysis, and optimization processes," *Structural and Multidisciplinary Optimization*, vol. 46, pp. 273–284, Aug. 2012.

[37] David, C., Delbecq, S., Defoort, S., Schmollgruber, P., Benard, E., and Pommier-Budinger, V., "From FAST to FAST-OAD: An open source framework for rapid Overall Aircraft Design," *IOP Conference Series Materials Science and Engineering*, vol. 1024, p. 012062, Jan. 2021.

[38] Gray, J. S., Hwang, J. T., Martins, J. R. R. A., Moore, K. T., and Naylor, B. A., "OpenMDAO: an open-source framework for multidisciplinary design, analysis, and optimization," *Structural and Multidisciplinary Optimization*, vol. 59, pp. 1075–1104, Apr. 2019.

[39] Kraft, D., *A software package for sequential quadratic programming*. Wiss. Berichtswesen d. DFVLR, 1988.

[40] "DT18 AG." delair.aero/wp-content/uploads/2017/03/DT18-AG-datasheet-1.2_WEB-1.pdf.

[41] "Lockheed Martin Hawk III."

[42] "Lockheed Martin Hawk IV."

[43] "EOS Strix 300." eos-technologie.com/en/mini-UAV-Strix-300.htm.

[44] "EOS Strix 400." eos-technologie.com/en/mini-UAV-Strix-400.htm.

[45] "Aeronautics Orbiter 2." aeronautics-sys.com/home-page/page-systems/page-systems-orbiter-2-mini-uas/.

[46] "Aeronautics Orbiter 3." aeronautics-sys.com/home-page/page-systems/page-systems-orbiter-3-stuas/.

[47] "BlueBird SpyLite." bluebird-uav.com/spylite-uav/.

[48] "AeroVironment Puma LE." avinc.com/uas/puma-le.

[49] "AeroVironment Puma 3 AE." avinc.com/uas/puma-ae.

[50] "AeroVironment Raven B." avinc.com/uas/raven.

[51] "AeroVironment Wasp AE." avinc.com/uas/wasp-ae.

[52] Verstraete, D., Palmer, J., and Hornung, M., "Preliminary Sizing Correlations for Fixed-Wing Unmanned Aerial Vehicle Characteristics," *Journal of Aircraft*, vol. 55, pp. 1–12, Sept. 2017.